Activation of a hybrid twinning mechanism in a Cr-Ni-Si-V-N medium manganese austenitic steel containing precipitates

S. Shyamal[a], M. Ghiasabadi Farahani[b], T. Allam[c,d], A.S. Hamada[e], C. Haase[c], J.I. Kömi[f], P.C. Chakraborti[g], P. Sahu[a,*]

[a] Department of Physics, Jadavpur University, Kolkata 700 032, India
[b] Hot Deformation and Thermomechanical Processing Laboratory of High-Performance Engineering Materials, School of Metallurgy and Materials Engineering, College of Engineering, University of Tehran, Tehran, Iran
[c] Steel Institute (IEHK), RWTH Aachen University, 52056 Aachen, Germany
[d] Department of Metallurgical and Materials Engineering, Suez University, 43528 Suez, Egypt
[e] Kerttu Saalsti Institute, University of Oulu, Pajatie 5, Nivala FIN-85500, Finland
[f] Centre for Advanced Steels Research, Box 4200, University of Oulu, FIN-90014 Oulu, Finland
[g] Department of Metallurgical and Material Engineering, Jadavpur University, Kolkata 700 032, India

article info

abstract

Twinning nucleation in a medium Mn austenitic steel containing precipitates is studied at low strain ~ 0.02, using transmission electron microscopy. In the near vicinity of the precipitates, unfaulting dis- location reaction is favored, while twinning is activated farther from the precipitates. Twin nucleation follows a hybrid mechanism, involving creation of stacking faults through classical dislocation dissoci- ation, while those stacking faults subsequently overlapped following a non-classical alternated stacking fault pair mechanism to create a three-layer twin nucleus. The observed twinning behavior is interpreted from an energy barrier variation viewpoint within the matrix.

Twinning is an important deformation mechanism in face-centered cubic (fcc) metals and alloys having low stacking fault energy (SFE), wherein pre-existing dislocation configurations dissociate into multi-layered stacking faults (SFs) forming a three- layer twin nucleus [1]. In classical models of twinning, sev- eral dislocation-based mechanisms exist concerning heterogeneous twin nucleation in fcc materials [1-5]. Twinning nucleate at sites of high local stress concentrations and is governed by several vari- ables, some of them interrelated, namely, composition, tempera- ture, strain rate, pre-strain, grain size and orientation, precipitates, etc. [1].

Depending on various length scales, i.e. the grain sizes, differ- ent twinning mechanisms are activated [1,6]. For instance, differ- ent dissociations of $^a(1\bar{1}0)$ dislocations are applicable in classi- cal methods when the grain sizes are above the nano crystalline (NC) regime [4,7-10]. The non-classical mechanisms are applicable to the NC regime involve emission of Shockley partial dislocations

(SPDs) from grain boundaries (GBs) [6,11,12] and alternated SF pair mechanism [13]. It is recently reported that a non-classical alter- nated SF pair twinning mechanism could be activated in grain sizes well above the NC regime [14].

The role of various parameters in controlling twinning behav- ior of fcc metals/alloys are widely reported, while its occurrence in presence of precipitates is poorly understood due to some conflict- ing reports. For instance, McHargue et al. [15] report that presence of precipitates would suppress twinning in Ti-Zr alloys. Yen et al. [16] also report that twins bypass the carbide precipitates in twin- ning induced plasticity (TWIP) steel, while Mahajan et al. [17] ob- served in Fe-Cr-Co alloy that micro-twins are formed during pre- cipitation hardening. Robson [18] further argued that precipitates would strongly suppress any twin growth, though his report con- cerns the hexagonal close packed (hcp) Mg-alloys.

Any precipitates in the matrix would result in a lattice mis- match between the precipitate and the matrix, and a local stress field in the surrounding matrix would develop [19]. In this report, we study the nucleation of deformation twinning, when the ma- trix contains stress fields induced by vanadium carbonitride, V(C,N) precipitates in a medium manganese (MMn) TWIP type steel. TWIP steels are known to exhibit profound twinning under straining, and

* Corresponding author. Jadavpur University, Dept. of Physics, Kolkata 700032, In- dia. Tel.: +919432958540, + 91–33–2457–2840, Fax: + 91–33–2413–7121
E-mail addresses: psahu74@gmail.com, psahu@phys.jdvu.ac.in (P. Sahu).
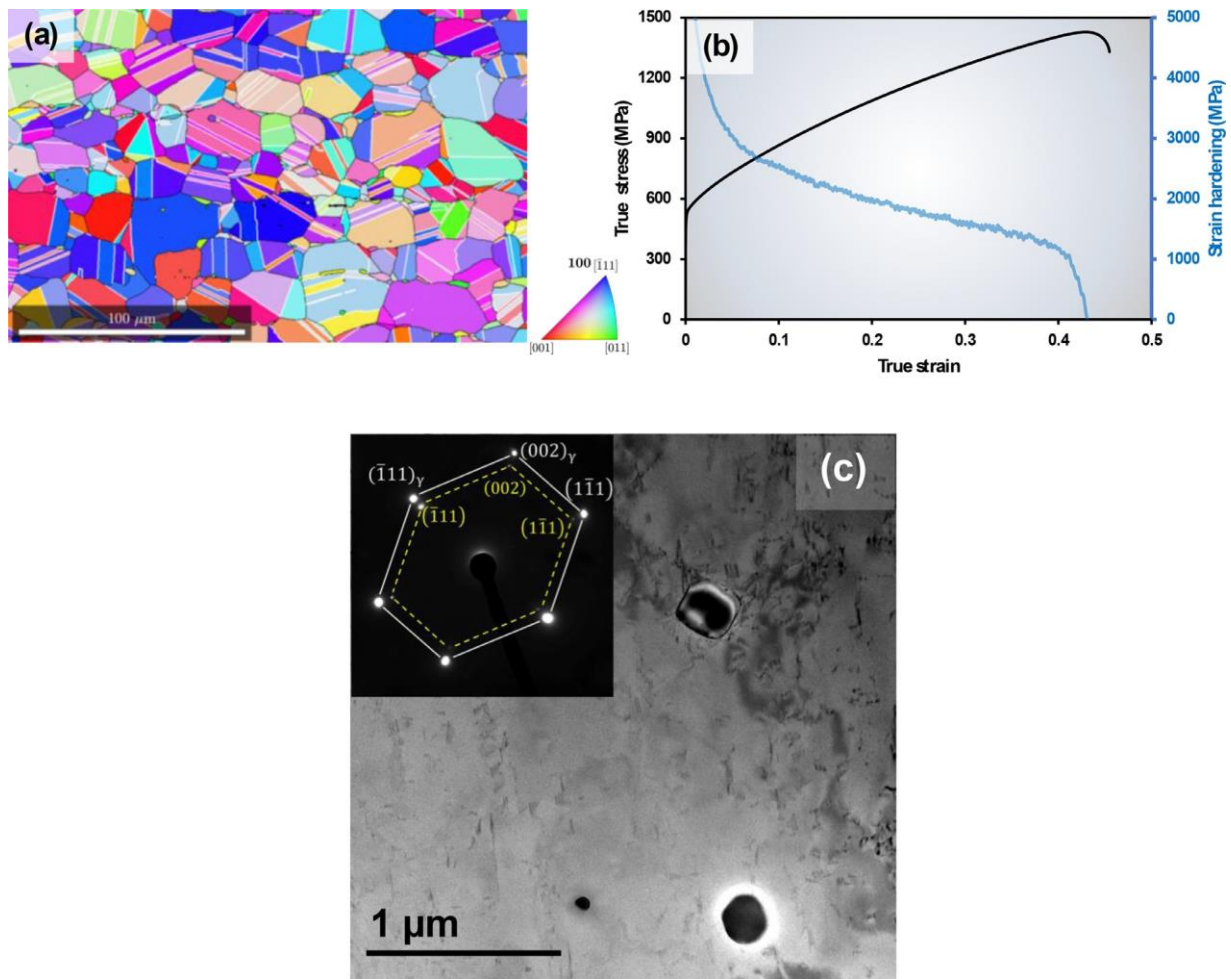
Fig. 1. (a) EBSD inverse pole figure map of the initial microstructure with average austenite grain size ≈ 20 μm (b) true stress-strain curve and superimposed strain hardening rate vs. true strain curve (c) low magnification TEM BF microstructure in the annealed undeformed condition. The inset shows an indexed $B \approx [01\bar{1}]$ SAD pattern of the matrix and precipitate in a cube-cube orientation: $[110]\gamma \parallel [110]_{V(C,N)}$.

the underlying twinning mechanisms are generally classical [5], while a non-classical mechanism is also reported [14]. The objective of this letter is to capture the emergence of twinning and the allied mechanism in presence of V(C,N) precipitation in austenitic MMn steel matrix.

The steel with composition Fe-0.17C-2.2Si-10.8Mn-18.0Cr-4.7Ni-0.9V-0.25N (wt.%) was ingot-cast, hot and cold rolled to a final thickness of 1.5 mm, followed by annealing heat treatment at 1200°C for 3 min. The annealing parameters were chosen from thermodynamic calculations to form only, V(C,N) precipitates [20]. The initial austenite microstructure (grain size ≈ 20 μm) displayed in Fig. 1(a) was obtained from an electron backscatter diffraction (EBSD) inverse pole figure map acquired with a 150 nm step size in Zeiss Sigma scanning electron microscope (SEM) at 20 kV, 30 nA. The twinning mechanism was identified using high-resolution transmission electron microscopy (HRTEM) in JEOL 2200FS elec- tron microscope on specimens deformed to 0.02 true strain. Tensile test was carried out at room temperature with strain rate: 10^{-3} s^{-1} on A30 specimens of 30 mm gauge length and 6 mm width.

The tensile flow behavior and the strain hardening rate (SHR) of the steel are superimposed in Fig. 1(b). The steel has a high initial SHR of ~ 3.9 GPa, gradually decreasing to ~ 1.37 GPa, until a true strain of 0.37. The V(C,N) precipitate in the microstructure is confirmed from the indexed $B \approx [01\bar{1}]$ selected area diffraction (SAD) pattern corresponding to the low magnification bright field (BF) TEM micrograph in Fig. 1(c). The V(C,N) precipitates here have

sizes between: 160-290 nm with a V content varying between: 65-70% (wt. %), determined by energy dispersive X-ray spectroscopy unit integrated with the TEM, and they have a cube-cube orien- tation relationship with the austenite matrix [21]. The precipitates in this steel are significantly larger than those observed by Kwon et al. [21], while cementite remained absent. This is attributable to the relatively higher annealing temperature and time used in the present study, besides the major differences in steel chemical com- position, namely, C, Si and Cr contents. The precipitates in Fig. 1(c) are also not surrounded by significant dislocations, unlike in the deformed state; discussed below.

A set of BF TEM microstructures at true strain: 0.02 presented in Fig. 2, reveal a high density of forest dislocations surround the precipitates, whose comparison with Fig. 1(c) indicate that the dislocation clusters observed around the precipitates in Fig. 2 are presumably formed during the course of deformation. It will be shown that the associated stress fields have had different consequences on the microstructure evolution. On one hand, a couple of arrows in- dicate a dislocation pile-up (DP) in Fig. 2(a) traversing the matrix in the vicinity of the precipitation. It is further seen in Fig. 2(a) that as one moves away from the precipitate, the characteristic SF fringe contrast becomes prominent in the pile-up, and indicated by white arrow. In contrast, the fringed region (*i.e.* the SF) is narrowed down gradually near the tip of the pile-up, and finally disappears. This is synonymous to conversion of partial dislocations to perfect dislocations near the precipitate (yellow arrow).
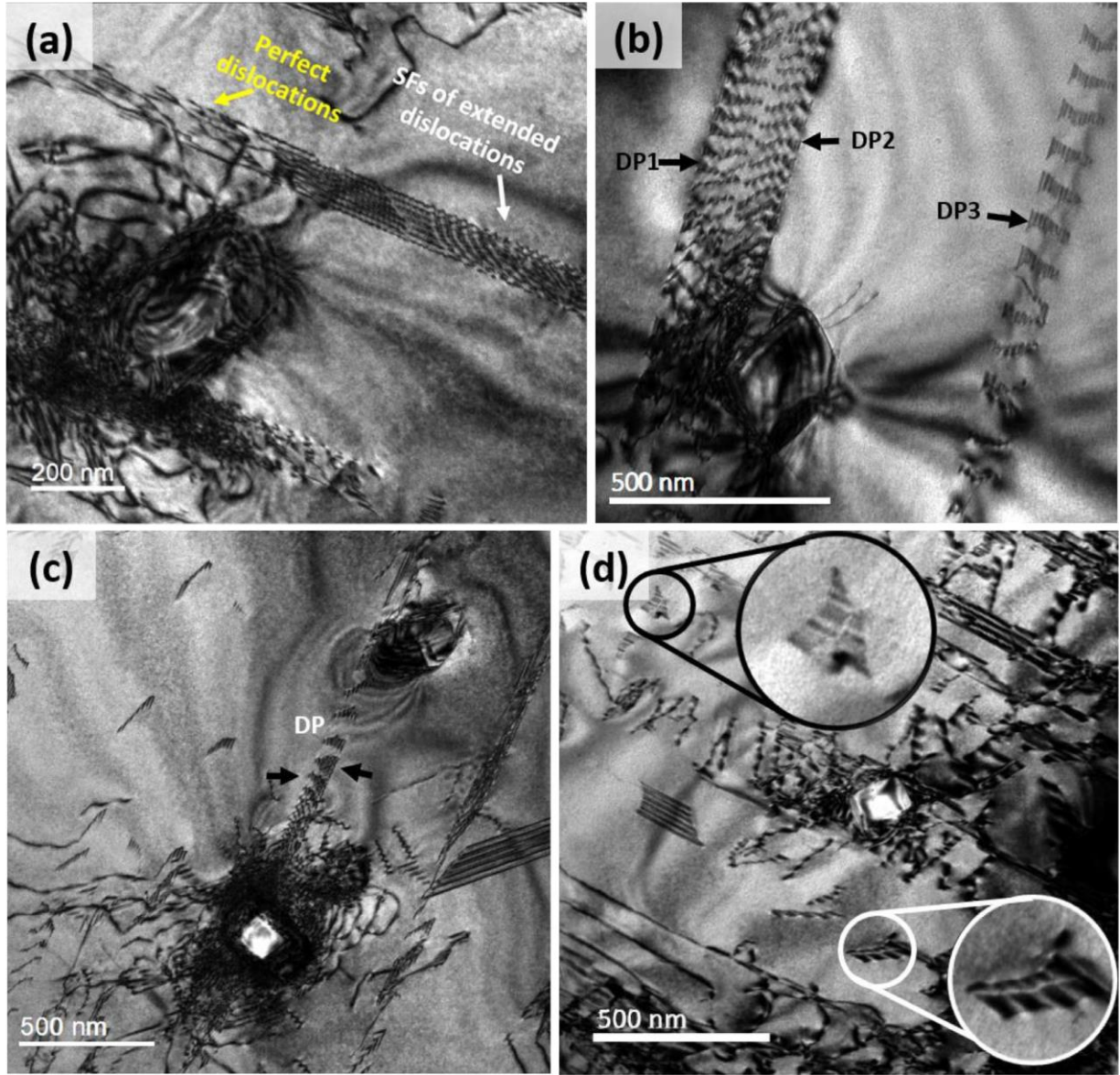
Fig. 2. TEM BF microstructure at true strain: 0.02: (a) extended and full dislocations surrounding a precipitate are indicated using white and yellow arrows, respectively. (b) dislocation pile-ups (DPs) observed at different distances from a precipitate (c) nucleation of SFs in a DP is indicated using black arrows (d) nucleation of three-layer twin nuclei, away from the precipitates are encircled and magnified.

The present steel has a low intrinsic SFE, $\gamma_{isf} \sim 25$ mJ/m^2, calculated using a sub regular solution model [22]. Any SF removal in Fig. 2(a) is a result of the following unfaulting dislocation reaction that occurs under high SFE conditions, and represented in Thompson tetrahedron notation as [23]:

$$B\alpha + \alpha A \rightarrow BA \tag{1}$$

The high SFE here does not refer to the global SFE of the steel, rather to the local high value near the precipitates, which is based on the concept of effective SFE arising from interaction between SF and the stress field of dislocations [24]. The removal of SF (Eq. (1)) near the vicinity of the precipitate observed in Fig. 2(a) is fur- ther evidenced in Fig. 2(b), wherein, three independent DPs are detected at different distances from the precipitate. DP1 and DP2 lie close to the precipitate, while DP3 is relatively farther from it. It is additionally discernible in Fig. 2(b) that the SFs in DP1 and DP2 are narrower than the ones in DP3, and that the glide of dis- locations in DP1 and DP2 ceases as they approach the precipitate, while continuing in DP3. Interestingly, despite the steel having a

low γ_{isf}, the microstructures in Fig. 2 reveal that the SFs observed are significantly narrower, but not infinitely long as observed in TWIP steels deformed to low strain [5], and the reasons thereof will be assessed subsequently.

Fig. 2(c) further captures a DP located in between two reason- ably separated precipitates. The width of any SF created by the ex- tended dislocations in the pile-up of Fig. 2(c) is maximum when it is equidistant from both the precipitates (indicated by a pair of black arrows), since the net stress field effect is minimum at the mid position of the DP. Thus, it is likely that the dislocation substructure around the precipitate locally raises the critical stress for the glide of dislocations, and therefore leads to the unfault- ing reaction in Eq. (1). Fig. 2(d) demonstrates the first incidence of twin nuclei *i.e.* three-layer SFs, which are encircled. Such three- layer SF twin nucleus under two-beam dynamical conditions reveal a characteristic periodic contrast, which is reported in several stud- ies [5,25,26], and that these SF pairs continue to grow one above another to yield a macroscopic twin lamella [26].
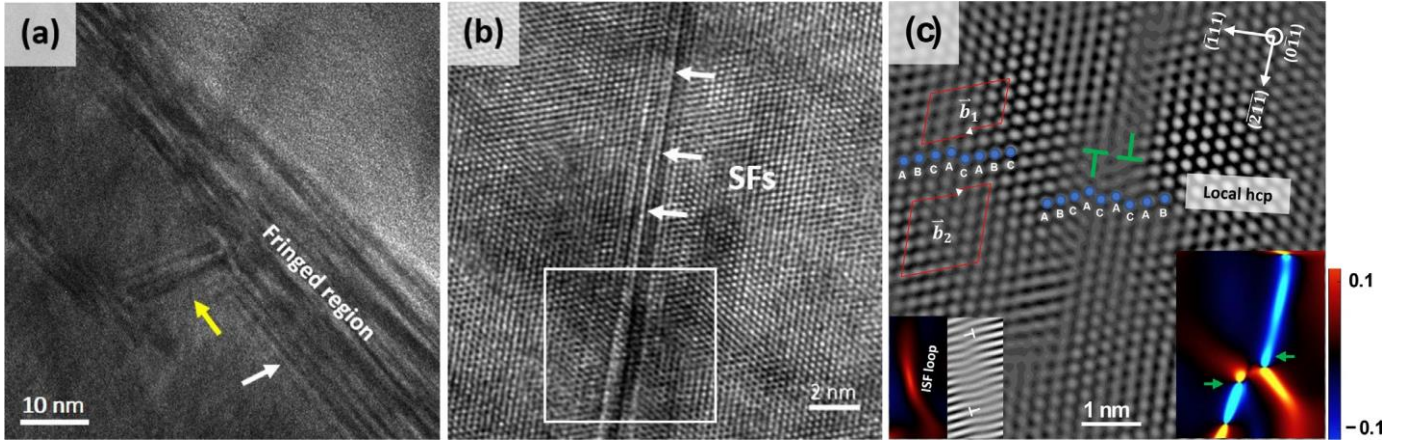
Fig. 3. HRTEM microstructure at true strain: 0.02: (a) fringed region serving as twinning precursors through alternated SF pairs in two different slip systems indicated by black and yellow arrows (b) higher magnification image of SFs along $B \approx [01\bar{1}1]$ (c) IFFT image of the white delineated region (b), Frank partials produced according to Eq. (2) are labeled as green "$\perp$". An ISF loop is also bound by two Shockley partials having opposite Burgers vectors (b_1 and b_2). The g-map and filtered IFFT image of the left lower inset shows that the ISF loop is bound by two 30° Shockley partials having opposite Burgers vectors: $\frac{a}{6}[2\bar{1}\bar{1}]$ and $\frac{a}{6}[211]$. The g-map from the local hcp region (middle region) along $[2\bar{1}\bar{1}]$ is shown in right lower inset. The indigo and yellow legends therein, respectively indicate the maximum compressive and tensile strains around the partial and full dislocations in the region.
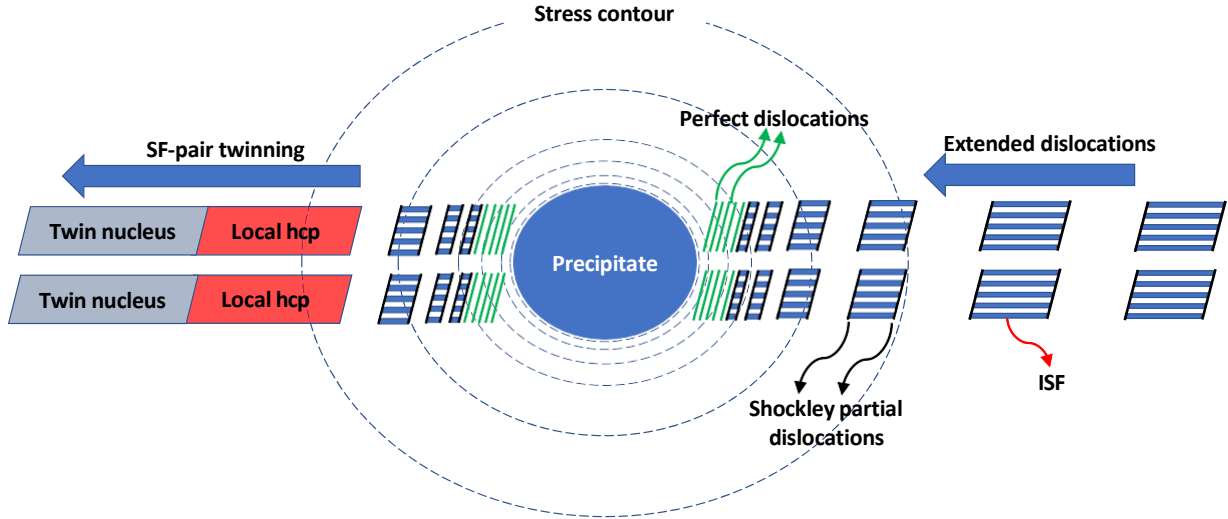
Fig. 4. Schematic illustrations of comprehensive picture of microstructure evolution due to presence of precipitate.

Dislocation slip and twinning are competitive mechanisms in coarse-grained (CG) metals/alloys, and a critical dislocation activity is required before the deformation twins can nucleate [27]. In contrary, the onset of twinning in NC cases occurs through various GB mediated mechanisms, involving emission and/or glide of SPDs, leaving behind intrinsic stacking faults (ISFs) [6,13,28-31]. However, the microstructures presented in Fig. 2 revealed clearly that any activities of $\frac{a}{2}\langle 110 \rangle$ dislocations, other than the unfaulting reaction Eq. (1) were not prevalent at 0.02 strain, even though twins clearly nucleate at this strain (Fig. 2(d)). This opens up the question about the twinning mechanism active here; in absence of any significant

perfect dislocation activity. To resolve this issue, we focus on two aspects; firstly, how the SFs are created in the course of deformation, secondly, their sequential overlapping on successive {111} planes so that the combination is regarded as a twin nucleus.

The HRTEM investigations and the corresponding inverse fast Fourier transform (IFFT) analysis presented in Fig. 3 helped resolving these two aspects. In Fig. 3(a), a fringed region is observed

within the austenite matrix, arising from SFs with at least one atomic

presented in Fig. 3(b) strengthens the argument about incidence of overlapped one atomic layer SF regions within the microstructure and that such prevalence was not sporadic in nature. The corresponding IFFT image of the delineated region of Fig. 3(b) presented in Fig. 3(c) reveals some even interesting propositions, discussed below.

Fig. 3(c) shows local g-maps, revealing the individual dislocations, based on an image processing technique [32]. The g-map and filtered IFFT image in the lower left inset of Fig. 3(c) allows identifying two 30° mixed leading Shockley partial loops without the trailing loops, having opposite Burgers vectors: $\frac{a}{6}[2\bar{1}\bar{1}]$ and $\frac{a}{6}[211]$.

The generalized SFE theory [33] for fcc metals suggest that when an ISF is formed due to passage of the leading partial, the trailing partial needs to overcome an energy barrier, which is a function of the ratio of unstable to intrinsic SFEs, γ_{usf} and γ_{isf}, respectively. It is also proposed that partials are expected for: $\frac{\gamma_{usf}}{\gamma_{isf}} \gg 1$, while

no dissociation should occur for: $\frac{\gamma_{usf}}{\gamma_{isf}} \approx 1$ [33]. The γ_{usf} value of

layer distance, rather, an alternated SF pair, being a twin precursor in non-classical twinning method [14]. The lattice image

the steel based on a previous study [14] was approximated ~ 280 mJ/m², relying on the assumption that γ_{usf} is so large in compar-

ison to γ_{isf} (~ 25 mJ/m^2) that any effect of additional alloying elements on the ratio would be insignificant. It is reported that γ_{usf} in γ-iron remains largely unaffected by Mn variations [34,35]. This argument leads to a high value of $\frac{\gamma_{usf}}{\gamma_{isf}} \approx 11$ in the present steel, implicating that dislocation dissociation should occur here. Since experimental determinations of the generalized SFEs are not possible, and therefore, the literature values are adapted to interpret the deformation microstructure.

A further observation from the middle region of the IFFT in Fig. 3(c) is the formation of two ISFs identified on the basis of stacking sequence: $ABCA/CA/CAB$, representing a local hcp struc- ture, which is synonymous to an alternated SF pair region. The g- map from this region of Fig. 3(c) in $[2^-\,1^-\,1^-]$ direction as shown in the lower right inset, additionally indicates the presence of Frank partials (green "⊥"s in Fig. 3(c)), which allows to understand that the alternated SF pair representing the local hcp region is most likely formed through dissociation of a $\frac{a}{2}\langle 110 \rangle$ perfect dislocation following the reaction:

$$\frac{a}{2}[011] \rightarrow \frac{a}{6}[211] + \frac{a}{3}\overline{1}11 \tag{2}$$

The presence of dissociated lattice dislocations and ISF loops in Fig. 3(c) directly indicate that away from the precipitates in the matrix, dissociation of $\frac{a}{2}\langle 110 \rangle$ dislocations should occur due to high value of the $\frac{\gamma_{usf}}{\gamma_{isf}}$ ratio ~ 11, while their associated stress field modify the energy barriers near the precipitates, and a consequent increase in γ_{isf} in their vicinity would result in lowering the $\frac{\gamma_{usf}}{\gamma_{isf}}$ value from its actual value. Consequently, the dissociation of $\frac{a}{2}\langle 110 \rangle$ dislocations in their immediate neighborhood would be prevented (Fig. 2). On the other hand, the prevalence of local hcp structures in Fig. 3 indicates that alternated SF pair mechanism, being non-classical in nature, is also operating here. In this mech- anism, a third ISF nucleates in between the previously formed al- ternated SF pair to subsequently convert it into a three-layer twin [13].

The nucleation of a trailing partial requires the energy barrier, $\gamma_{usf} - \gamma_{isf}$ to be overcome [36], and its absence in Fig. 3(c) should therefore be attributed to mismatch of this energy barrier. Since the energy barrier; $\gamma_{usf} - \gamma_{isf}$ is gradually lowered towards the precipitate due to local elevation of γ_{isf}, this situation would suppress any twin formation there since the nucleation of a second leading SPD on the second atomic plane is not favored, as would be the SF formation. The microstructures in Fig. 2 also strengthen this conjecture that SF formation in the vicinity of precipitates is quite unlikely in such instances due to high local γ_{isf}. The unfault- ing reaction in Fig. 2(c) reaffirms that SF formation is not preferred near the precipitates, where the local γ_{isf} is relatively higher. It is worth mentioning that V(C,N) precipitation would cause a local C depletion in the matrix, and consequent lowering of local γ_{isf}. It is however, reported that experimentally determined γ_{isf} value in Fe-Mn-Si-Al steels containing simple dislocation substructures can manifest more than two-fold increase due to its interaction with SFs [26]. Therefore, it is reasonable to expect that any drop in γ_{isf} due to C depletion would be overwhelmed by the disloca- tions' stress field effect on the SFs.

In classical theory, equilibrium width of SF depends only on γ_{isf} [37], and it cannot explain the finer SFs observed in Fig. 2, despite the steel possessing a low γ_{isf} ~ 25 mJ/m^2. This however, could be explained by modern dislocation dynamics studies for NC fcc metals that the equilibrium width depends not on γ_{isf} alone,

spectively [33]. The equilibrium SF width directly influences the deformation mechanism, particularly in NC metals, and that the width depends on – grain size, temperature and applied stresses [38,39]. The prevalence of narrower SFs in Fig. 2 indeed advocates according to Hunter et al. [38] that the barrier: $\gamma_{usf} - \gamma_{isf}$ in the present steel is effectively lowered from its calculated value: (280 − 25) mJ/m$^2 \approx 255$ mJ/m^2 to inhibit any widening of SFs. At the same time, the multitude of SFs in Fig. 2 and the fringed region in Fig. 3(a) would further ensure that twins should nucleate through overlap of SFs once the energy barrier is surpassed, while the ac- tivation of non-classical alternated SF pair mechanism is ascribed to the $\frac{\gamma_{usf}}{\gamma_{isf}}$ ratio [13,14]. The active deformation mechanism of the microstructure is schematically presented in Fig. 4.

In hindsight, the low strained (0.02) microstructure of a medium Mn steel containing V(C,N) precipitates reveals that stack- ing faults and twins were not observed in immediate vicinity of the precipitate due to the surrounding high stress field modify- ing the energy barrier for nucleation of these faults. They are ob- served farther from the precipitates. Twinning occurred through a hybrid mechanism, wherein, the stacking faults are created follow- ing a classical dislocation dissociation, while those stacking faults overlap to create a three-layer twin following a non classical route, explicable through unstable to intrinsic stacking fault energies ra- tio of the steel ($\approx$ 11).

Declaration of Competing Interest

The authors further declare no conflict of interests and that all the funding agencies have been properly acknowledged.

Supplementary materials

Supplementary material associated with this article can be found, in the online version, at doi:10.1016/j.scriptamat.2020.10. 011.

References

[1] J.W. Christian, S. Mahajan, Prog. Mater. Sci. 39 (1995) 1–157.
[2] A. Ookawa, J. Phys. Soc. Japan 12 (1957) 825.
[3] J.A. Venables, Philos. Mag. 30 (1974) 1165–1169.
[4] M. Niewczas, G. Saada, Philos. Mag. A 82 (2002) 167–191.
[5] B. Mahato, T. Sahu, S.K. Shee, P. Sahu, T. Sawaguchi, J. Kömi, L.P. Karjalainen, Acta Mater. 132 (2017) 264–275.
[6] Y.T. Zhu, X.Z. Liao, X.L. Wu, Prog. Mater. Sci. 57 (2012) 1–62.
[7] S. Mahajan, G.Y. Chin, Acta Metall. 21 (1973) 1353–1363.
[8] M. Niewczas, Dislocations in Solids 13 (2007) 263–364.

[9] J.A. Venables, Philos. Mag. 6 (1961) 379–396.
[10] J.A. Venables, J. Phys. Chem. Solids 25 (1964) 685–692.

but on the energy barrier, $\gamma_{usf} - \gamma_{isf}$, which must be overcome for any widening of SFs [38]. Therefore, the deformation mechanism

in the present steel is now introspected from a NC metal/alloy viewpoint. It is known that narrower SFs are expected in NC Cu and Al having $\gamma_{usf} - \gamma_{isf}$ values: 122 mJ/m² and 28 mJ/m², re-

[11] Y.T. Zhu, X.Z. Liao, X.L. Wu, JOM 60 (2008) 60–64.
[12] V. Yamakov, D. Wolf, M. Salazar, S.R. Phillpot, H. Gleiter, Acta Mater. 49 (2001) 2713–2722.
[13] L. Wang, P. Guan, J. Teng, P. Liu, D. Chen, W. Xie, D. Kong, S. Zhang, T. Zhu, Z. Zhang, E. Ma, M. Chen, X. Han, Nat. Commun. 8 (2017) 1–7.
[14] M. Ghiasabadi Farahani, A. Zarei-Hanzaki, H.R. Abedi, J.H. Kim, M. Jaskari, P. Sahu, L.P. Karjalainen, Scr. Mater. 178 (2020) 301–306.
[15] C.J. McHargue, H.E. McCoy, Amer. Inst. Min. Eng. 227 (1963) 1170.
[16] H.-W. Yen, M. Huang, C.P. Scott, J.-R. Yang, Scr. Mater. 66 (2012) 1018–1023.

[17] S. Mahajan, S. Jin, D. Brasen, Acta Metall. 28 (1980) 971–977.

[18] J.D. Robson, Acta Mater. 121 (2016) 277–287.

[19] W. Tirry, D. Schryvers, Acta Mater. 53 (2005) 1041–1049.

[20] T. Allam, X. Guo, S. Sevsek, M. Lipin´ska-Chwałek, A. Hamada, E. Ahmed, W. Bleck, Metals (Basel). 9 (2019) 705.

[21] Y. Kwon, A. Zargaran, J.H. Ryu, N.J. Kim, Scr. Mater. 172 (2019) 125–129.

[22] A.T. Dinsdale, Calphad 15 (1991) 317–425.

[23] D. Hull, D.J. Bacon, Introduction to Dislocations, Fifth Edition, Butter-worth-Heinemann, Oxford, 2011.

[24] P. Müllner, P.J. Ferreira, Philos. Mag. Lett. 73 (1996) 289–298.

[25] J.-K. Kim, M.-H. Kwon, B.C. De Cooman, Acta Materialia 141 (2017) 444–455.

[26] B. Mahato, S.K. Shee, T. Sahu, S. Ghosh Chowdhury, P. Sahu, D.A. Porter, L.P. Karjalainen, Acta Mater. 86 (2015) 69–79.

[27] E. El-Danaf, S.R. Kalidindi, R.D. Doherty, Metall. Mater. Trans. A 30 (1999) 1223–1233.

[28] L. Wang, J. Teng, P. Liu, A. Hirata, E. Ma, Z. Zhang, M. Chen, X. Han, Nat. Com-mun. 5 (2014) 4402.

[29] L. Wang, X. Han, P. Liu, Y. Yue, Z. Zhang, E. Ma, Phys. Rev. Lett. 105 (2010) 135501.

[30] D.H. Warner, W.A. Curtin, S. Qu, Nat. Mater. 6 (2007) 876–881.

[31] L. Wang, J. Teng, X. Sha, J. Zou, Z. Zhang, X. Han, Nano Lett. 17 (2017) 4733–4739.

[32] M.J. Hÿtch, J.-L. Putaux, J.-M. Pénisson, Nature 423 (2003) 270–273.

[33] Z.H. Jin, S.T. Dunham, H. Gleiter, H. Hahn, P. Gumbsch, Scr. Mater. 64 (2011) 605–608.

[34] D.W. Boukhvalov, Y.N. Gornostyrev, M.I. Katsnelson, A.I. Lichtenstein, Phys. Rev. Lett. 99 (2007) 247205.

[35] N.G. Kioussis, N.M. Ghoniem, J. Comput, Theor. Nanosci. 7 (2010) 1317–1346.

[36] J.R. Rice, J. Mech, Phys. Solids 40 (1992) 239–271.

[37] J.P. Hirth, J. Lothe, Theory of Dislocations, McGraw-Hill, NewYork, 1968.

[38] A. Hunter, R.F. Zhang, I.J. Beyerlein, T.C. Germann, M. Koslowski, Model. Simul. Mater. Sci. Eng. 21 (2013) 25015.

[39] H. Van Swygenhoven, P.M. Derlet, A.G. Frøseth, Nat. Mater. 3 (2004) 399–403.